RESEARCH ACTIVITIES II
Department of Molecular Structure

II-A Laboratory and Astronomical Spectroscopy of Transient Molecules

Vast, cold, and low-density space environment is a unique laboratory, whose physical and chemical conditions are rarely attained in the laboratory on Earth. The unique space laboratory is favorable to the existence of transient molecules such as molecular ions, free radicals, and unstable molecules, most of which are very exotic and nonterrestrial. These exotic transient molecules are generally difficult and challenging problems for laboratory spectroscopy. Laboratory spectroscopy may be enriched by astronomical studies on non-terrestrial transient species which represent new developments in high-resolution molecular spectroscopy. On the other hand, detailed knowledge about new transient molecules obtained by laboratory spectroscopy is essential to a deeper understanding of physical and chemical processes in space. We developed a high-sensitivity submillimeter-wave and far-infrared spectrometers suitable for high-resolution spectroscopy of transient molecules of astronomical interest. We expect that our laboratory spectroscopy may accelerate the mutually beneficial aspect between laboratory spectroscopy, and astrochemistry and astrophysics.

II-A-1 The detection of the Free Radical FO ($X^2\Pi_{3/2}$) by Microwave Spectroscopy

TAMASSIA, Filippo[1]; BROWN, John M.[2]; SAITO, Shuji
([1]Oxford Univ. and IMS; [2]Oxford Univ.)

The FO radical is the most fundamental halogen oxide free radical and has been studied since 1979 by high-resolution infrared spectroscopy, CO_2-LMR spectroscopy,[1)] diode laser spectroscopy[2)] and Fourier transform IR spectroscopy.[3)] A full spectroscopic characterization has been recently achieved with the detection of the fine-structure transition $^2\Pi_{1/2}$–$^2\Pi_{3/2}$ by FIR-LMR.[4)] No pure rotational spectra have been reported in literature to date. McKellar,[5)] in a Stark spectroscopy experiment, demonstrated that the electric dipole moment is exceptionally small, *i.e.* 0.0043(4) D for the $v = 0$ level and 0.0267(9) D for $v = 1$.

We detected for the first time the pure rotational spectrum of the free radical FO ($X^2\Pi_{3/2}$) by microwave spectroscopy, using a reaction of ozone with atomic fluorine. Four rotational transitions $J = 7/2$–$5/2$ to 13/2–11/2 have been measured in the frequency region 219–408 GHz. All the observed transitions are magnetic dipole in character. No electric dipole transitions have been observed in this experiment. Each rotational transition is split into four components by fluorine magnetic hyperfine interaction ($I_F = 1/2$) and by Λ-type doubling. The analysis of the observed data allowed a considerable improvement of some spectroscopic parameters: $B_0 = 31539.33542(32)$ MHz.

References
1) A. R. W. McKellar, *Can. J. Phys.* **57**, 2106 (1979).
2) A. R. W. McKellar, C. Yamada and E. Hirota, *J. Mol. Spectrosc.* **97**, 425 (1983).
3) J. B. Burkholder, P. D. Hammer, C. J. Howard and A. R. W. McKellar, *J. Mol. Spectrosc.* **118**, 471 (1986).
4) F. Tamassia, J. M. Brown and K. M. Evenson, *J. Chem. Phys.* **110**, 7273 (1999).
5) A. R. W. McKellar, *J. Mol. Spectrosc.* **101**, 186 (1983).

II-A-2 Microwave Spectroscopic Detection of Transition Metal Hydroxide: CuOH and AgOH

WHITHAM, Christopher J.[1]; OZEKI, Hiroyuki; SAITO, Shuji
([1]Oxford Univ. and IMS)

[*J. Chem. Phys.* **110**, 11109 (1999) and *ibid.* in press]

A number of microwave spectroscopic studies on metal hydroxide molecules have been reported: alkali metal hydroxides NaOH to CsOH, alkali earth metal hydoxides MgOH to BaOH, and recently, AlOH and InOH. Linearity or nonlinearity of the metal hydroxides depend on a balance between ionic and covalent structures.[1)] In contrast, there has been no previous microwave spectroscopy of transition metal hydroxides, where a contribution of d orbital in transition metal influences the balance between both structures. There is a need for microwave spectroscopy of such molecules, which can supply substantial information on this problem through their structural determination.

We detected rotational spectra of CuOH and AgOH for the first time by milimmetr- and submillimeter-wave spectroscopy (see Figure 1). Both molecules were directly produced in the hollow cathode discharge cell by sputtering metal from the hollow cathode made of the corresponding metal, and showed asymmetric-top a-type R-branch transitions. The deuterated species CuOD and AgOD were also observed by using D_2O adsorption on the electrode in advance of measurements. From the observed molecular constants for isotopic species of both molecules their harmonic force field and zero-point averaged (r_z) structures were derived and discussed in terms of the balance between competing ionic and covalent interactions.

References
1) C. W. Bauschlicher, S. R. Langhoff and H. Partridge, *J. Chem. Phys.* **84**, 901 (1986).

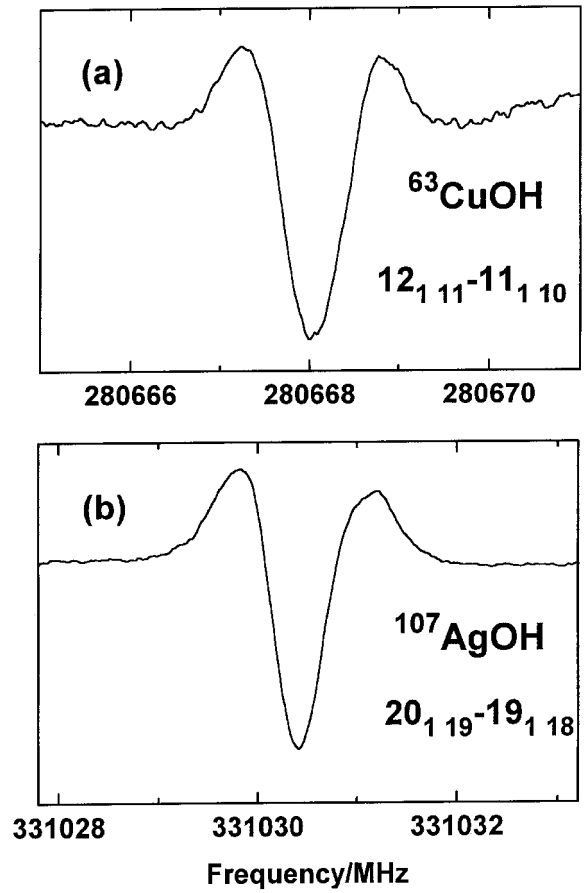

Figure 1. (a) The $12_{1,11}$-$11_{1,10}$ transition of ^{63}CuOH observed in a discharge cell, with a copper hollow cathode. (b) The $20_{1,19}$-$19_{1,18}$ transition of ^{107}AgOH observed with silver sheets inserted inside a stainless steel hollow cathode.

II-A-3 Microwave Spectrum of the Inversion-Rotation Transition of the D_3O^+ Ion: $\Delta k = \pm 3n$ Interaction and Equilibrium Structure

ARAKI, Mitsunori[1]; OZEKI, Hiroyuki; SAITO, Shuji
([1]GUAS)

[*Mol. Phys.* **97**, 177 (1999)]

In the last Annual Review we reported the experimental determination of the ground-state inversion splitting in D_3O^+ by microwave spectroscopy.[1)] We further measured 28 Q-branch lines including $J = K + 5$ in the 399–458 GHz region and analyzed them with previously measured R-branch and Q-branch lines, 53 lines in total. We found that inclusion of $\Delta k = \pm 3n$ interactions in the Hamiltonian was essential for a full explanation of the observed lines, with measurement uncertainty of 20 to 60 kHz. The molecular constants, including C for the 0^+ and 0^- levels, as well as the $\Delta k = \pm 3n$ interaction parameters, were derived from the fit of all data. The inversion splitting was determined to be 15.35550338(107) cm^{-1}, where the number in paprentheses denote one standard deviation of the fit. Zero-point corrections to the rotational constants of H_3O^+ and D_3O^+ were calculated from a harmonic potential of H_3O^+ and the r_z structures were derived from the zero-point corrected rotational constants:

$D_3O^+(0^+)$: $r_z = 0.9818(23)$ Å, $\theta_z = 112.68(100)°$,
$D_3O^+(0^-)$: $r_z = 0.9830(23)$ Å, $\theta_z = 112.02(100)°$.

From the shift between the r_z structures of H_3O^+ and D_3O^+ the equilibrium structural parameters of H_3O^+ was estimated to be $r_e = 0.9702(89)$ Å, $\theta_e = 109.4(38)°$.

References

1) M. Araki, H. Ozeki and S. Saito, *J. Chem. Phys.* **109**, 5707 (1998) and *Annu. Rev.* II-A-5 (1998).

II-B Laser Cooling and Trapping of Neutral Atoms

When atoms absorb or emit photons, the atoms are accelerated or decelerated because photons have momenta. On the other hand, a strong radiation field modifies the internal energy of an atom, so that an atom in an inhomogeneous radiation field receives a force from the field. The former mechanism allows us to decrease the translational temperature of neutral atoms down to an extremely low temperature by means of laser radiation, and the latter enables the spatial control of neutral atoms with lasers. As the translational temperature goes down to the nano kelvin region, the atomic de Broglie wavelength becomes a macroscopic size and some macroscopic quantum-mechanical collective motion of atoms can then be expected to occur. Such a long de Broglie wavelength also enables us to realize the atomic interferometry. On the other hand, easy control of the atomic spatial position and velocity with lasers is expected to open the possibility of various applications. For these reasons, we have been studying the laser cooling and trapping of neutral atoms.

II-B-1 Quantum Statistical Effects in Ultracold Ionizing Collisions between Spin-Unpolarized Metastable He($2s^3S_1$) Atoms

KUMAKURA, Mitsutaka; MORITA, Norio

[*Phys. Rev. Lett.* **82**, 2848 (1999)]

We have carried out a precise theoretical investigation on the cause of the isotopic difference in collisional ionization rate coefficients between cold ^{4}He($2s^3S_1$) + ^{4}He($2s^3S_1$) and ^{3}He($2s^3S_1$) + ^{3}He($2s^3S_1$) collisions at 0.5 mK, which is observed in our previous magneto-optical trap experiments on He atoms. The rate coefficients experimentally obtained for ^{4}He-^{4}He and ^{3}He-^{3}He collisions are $(3.8 \pm 1.1) \times 10^{-10}$ cm^3/s and $(1.1 \pm 0.4) \times 10^{-9}$ cm^3/s, respectively, and there is a large isotopic difference of a factor of 3 between them. Through our theoretical calculation, we have found that this difference is an explicit manifestation of the differing quantum statistics of those isotopes: at such a low temperature, the ionization process is mainly caused by only a single scattering partial wave (*s*-wave). Therefore, the electronic states that can contribute to the ionization explicitly differ between ^{4}He-^{4}He and ^{3}He-^{3}He collisions because of the differing quantum statistical symmetries of the isotopes. This is the main reason why there is a large isotopic difference in the ionization rate coefficients. Our calculation, which is based on this consideration and takes into account not only the spin conservation rule in the ionization process but also a small contribution of the *p*-wave tunneling through its centrifugal barrier, has given the rate coefficients of 2.2×10^{-10} cm^3/s and 1.0×10^{-9} cm^3/s for ^{4}He-^{4}He and ^{3}He-^{3}He collisions, respectively. These values agree well with the experimental results. It is interesting that the rate coefficient for the fermionic isotope (^{3}He) is larger than for the bosonic one (^{4}He), which is just contrary to the results of similar experiments on cold ionizing collisions of spin-polarized Kr[1] and Xe[2] atoms. From our calculation, we have found that this is because the spin conservation rule holds good in He atoms while in heavier rare gas atoms it breaks down. An optical enhancement of the collisional ionization is also observed in our previous experiment on the cold atomic collision irradiated with trap laser beams. Our theoretical values are in good agreement with the experimental results, and this enhancement has been attributed to the fact that in the presence of the laser irradiation many partial waves up to the 6-th order can contribute to the ionization. We have also found that this fact results in the smaller isotopic difference in the enhanced ionization rates.

References

1) H. Katori, H. Kunugita and T. Ido, *Phys. Rev. A* **52**, R4324 (1995).
2) C. Orzel, M. Walhout, U. Sterr, P. S. Julienne and S. L. Rolston, *Phys. Rev. A* **59**, 1926 (1999).

II-C Spectroscopy of Atoms and Ions in Liquid Helium

Ions and atoms in liquid helium are known to reside in bubble-like cavities due to the Pauli repulsive force between electrons. Physical properties in these exotic surroundings are determined by the potential energy of the impurity-He$_n$ system, the surface tension energy of the liquid helium, and the pressure-volume energy. Spectroscopic studies of ions in liquid helium are expected not only to give information on the structure and dynamics of the bubbles, but also to contribute to the study on the property of superfluid liquid helium. Moreover, if we can study ions distributed just below the liquid helium, it will be a new method for the experimental research on the low dimension plasma physics.

II-C-1 Spectroscopic Study of Alkali-Earth Atoms in Liquid ^{3}He

MORIWAKI, Yoshiki; MORITA, Norio

The comparison between spectra of atoms in liquid ^{3}He and ^{4}He can allow us to find interesting phenomena arising from differing quantum features of each liquid helium, such as the quantum statistics and fluidity (normal and super). From this viewpoint, we have measured some spectra of Mg and Ca in liquid ^{3}He. As a result, it has been found that (a) excitation spectra of both atoms in liquid ^{3}He are much narrower and their blue shifts are significantly smaller than the ones in

liquid ^{4}He, and that (b) there is a large isotope shift in the emission spectrum of Mg while such a shift is not observed for Ca. The smaller width and shift in each excitation spectrum can be explained by the difference in the number density and surface tension between liquid ^{3}He and ^{4}He: because of the smaller mass of ^{3}He, its wavefunction has a size larger than ^{4}He, so that the number density of ^{3}He should be smaller. Moreover, because of the difference in the quantum statistical symmetry, the surface tension of liquid ^{3}He is about one third of that of liquid ^{4}He at 1.4 K. These facts make the size of an atomic bubble much larger in liquid ^{3}He than in liquid ^{4}He (soft cage effect), so that perturbations by surrounding ^{3}He atoms is much weaker. This effect results in the smaller peak shift and spectral width in the excitation spectra for liquid ^{3}He. In the case of Mg, while its excitation spectrum for liquid ^{3}He is narrower than for liquid ^{4}He, the width of its emission spectrum is almost the same as the one in liquid ^{4}He. These facts result in that the emission and excitation spectra for liquid ^{3}He have almost the same widths, although such a situation is quite unusual and hardly seen in ordinary bubble spectra. This fact can be understood with a model of exciplex formation in the excited state, which is similar to the one previously introduced to explain the emission spectrum of Mg in liquid ^{4}He. This model also consistently explains the red shift of the peak position in the emission spectrum, since it just agrees with an isotope shift estimated from the molecular vibrations.

II-D Endohedral Metallofullerenes: New Fullerene Molecules with Novel Properties

Endohedral metallofullerenes (fullerenes containing metal atoms inside hollow carbon cage) have long attracted special interest as new spherical molecules with novel properties. Recent important progress has been marked by successful isolation and purification in macroscopic quantities. With the availability of such purified samples, it has been possible to investigate the electronic properties and chemical reactivities.

II-D-1 Endohedrally Metal-Doped Heterofullerenes: La@C_{81}N and La_2@C_{79}N

AKASAKA, Takeshi[1]; OKUBO, Shingo[2]; WAKAHARA, Takatsugu[2]; YAMAMOTO, Kazunori[3]; KOBAYASHI, Kaoru[4]; NAGASE, Shigeru[4]; KATO, Tatsuhisa; KAKO, Masahiro[5]; NAKADAIRA, Yasuhiro[5]; KITAYAMA, Yoshie[2]; MATSUURA, Kenji[6]
([1]IMS and Niigata Univ.; [2]Niigata Univ.; [3]PRN; [4]Tokyo Metropolitan Univ.; [5]Univ. Electro-Commun.; [6]JEOL)

[*Chem. Lett.* 945 (1999)]

The first evidence of the gas-phase formation of endohedrally La-doped azafullerene ions La@C_{81}N and La_2@C_{79}N was obtained by the fast atom bombardment mass fragmentation of the adducts, La@C_{82}(NCH_2Ph) and La_2@C_{80}(NCH_2Ph).

II-D-2 Isolation and Characterization of a Pr@C_{82} Isomer

AKASAKA, Takeshi[1]; OKUBO, Shingo[2]; WAKAHARA, Takatsugu[2]; YAMAMOTO, Kazunori[3]; KATO, Tatsuhisa; SUZUKI, Toshiyasu; NAGASE, Shigeru[4]; KOBAYASHI, Kaoru[4]
([1]IMS and Niigata Univ.; [2]Niigata Univ.; [3]PRN; [4]Tokyo Metropolitan Univ.)

A minor isomer of Pr@C_{82} (Pr@C_{82}-II) has been isolated with an efficient two-step HPLC method, accompanied with a major isomer (Pr@C_{82}-I). The isolated Pr@C_{82}-II was well identified as a stable endohedral metallofullerene molecule. Mass spectra of both isomers confirmed that they were Pr@C_{82}. Visible and near-IR absorption spectra, and cyclic and differential pulse voltammograms for Pr@C_{82}-II showed characteristic features different from those for Pr@C_{82}-I. Chemical derivatization of both isomers were also accomplished. These data reveal that Pr@C_{82}-II is a carbon-cage isomer of Pr@C_{82}-I.

II-E Structure and Function of Respiratory Terminal Oxidases

In the aerobic respiratory chain of *Escherichia coli*, there are structurally unrelated two terminal oxidases. A heme-copper oxidase, cytochrome *bo* is predominantly expressed under highly aerated growth conditions while an alternative oxidase, a putative heme-heme oxidase, cytochrome *bd*, is predominant under microaerobic conditions. Both oxidases catalyze the two-electron reduction of ubiquinol-8 and the four-electron reduction of dioxygen, whereas only cytochrome *bo* exhibits vectorial proton transport. However, only a little structural information has been given for these ubiquinol oxidases. To clarify the molecular mechanism of electron transfer, chemical reaction of dioxygen, and proton pumping in the two respiratory terminal oxidases, we utilize various molecular spectroscopic techniques (*e.g.*, resonance Raman, EPR, FTIR) in conjunction with methods of molecular biology and biochemistry.

II-E-1 Fourier-Transform Infrared Studies on Azide Binding to the Binuclear Center of the *Escherichia coli bo*-Type Ubiquinol Oxidase

TSUBAKI, Motonari[1]; MOGI, Tatsushi[2]; HORI, Hiroshi[3]
([1]IMS and Himeji Inst. Tech.; [2]Univ. Tokyo; [3]Osaka Univ.)

[*FEBS Lett.* **449**, 191 (1999)]

Azide-binding to the heme-copper binuclear center of *bo*-type ubiquinol oxidase from *Escherichia coli* was investigated with Fourier-transform infrared spectroscopy. Deconvolution analyses of infrared spectra of the azide ($^{14}N_3$)-inhibited air-oxidized form showed a major infrared azide antisymmetric stretching band at 2041 cm^{-1}. An additional band developed at 2062.5 cm^{-1} during a longer incubation. Isotope substitutions with terminally ^{15}N-labeled azides did not show a splitting of the major band, indicating that the geometry of the bound azide is mainly in a bridging configuration between high-spin heme *o* and Cu_B.[1,2] The band at 2062.5 cm^{-1} showed clear splittings upon substitution with the terminally ^{15}N-labeled azides, indicating the Cu_B^{2+}–N=N=N structure. Partial reduction of the oxidase with β-NADH in the presence of azide ($^{14}N_3$) caused an appearance of new infrared bands at 2038.5 (major) and 2009 (minor) cm^{-1}. The former band also showed clear splittings in the presence of the terminally ^{15}N-labeled azides, indicating that reduction of low-spin heme *b* alters the structure of the binuclear center leading to the Fe_o^{3+}–N=N=N configuration.[3]

References

1) Tsubaki, M., Mogi, T., Anraku, Y. and Hori, H., *Biochemistry* **32**, 6065 (1993).
2) Tsubaki, M., Matsushita, K., Adachi, O., Hirota, S., Kitagawa, T. and Hori, H., *Biochemistry* **36**, 13034 (1997).
3) Tsubaki, M., *Biochemistry* **32**, 164 (1993).

II-E-2 Fluoride-Binding to the oxidized *Escherichia coli bd*-Type Ubiquinol Oxidase Studied by Visible Absorption and EPR Spectroscopies

TSUBAKI, Motonari[1]; MOGI, Tatsushi[2]; HORI, Hiroshi[3]
([1]IMS and Himeji Inst. Tech.; [2]Univ. Tokyo; [3]Osaka Univ.)

[*J. Biochem.* **126**, 98 (1999)]

Cytochrome *bd*-type ubiquinol oxidase in the aerobic respiratory chain of *Escherichia coli* contains two hemes *b* (b_{558} and b_{595}) and one heme *d* as redox metal centers.[1] To clarify the structure of the reaction center, we analyzed the fully oxidized enzyme by visible and EPR spectroscopies using fluoride ion as a monitoring probe. The visible spectral changes upon fluoride-binding were typical of ferric iron-chlorine species, indicating heme *d* as a primary binding site. The negative peak at 645 nm in the difference spectrum indicates that heme b_{595} also provides the low-affinity fluoride-binding site. Fluoride-binding caused a complete disappearance from the EPR spectra of the low-spin signals ascribable to heme *d* and spectral changes in both rhombic and axial high-spin signals. After fluoride-binding, each component of the rhombic high-spin signal showed superhyperfine splitting arising from the interaction of the unpaired spin of the heme *d* iron with the nuclear magnetic moment of ^{19}F. The axial high-spin species was converted to a new rhombic high-spin species assignable to heme b_{595}-fluoride. The $g = 2$ component of this new species also gave ^{19}F-superhyperfine splitting. These results indicate that both heme *d* and heme b_{595} can coordinate with a fluoride ion with different affinities in the fully oxidized state.

Reference

1) Mogi, T., M. Tsubaki, H. Hori, H. Miyoshi, H. Nakamura and Y. Anraku, *J. Biochem. Mol. Biol. Biophys.* **2**, 79 (1998).

II-E-3 Azide- and Cyanide-Bindings to the *Escherichia coli bd*-Type Ubiquinol Oxidase Studied by Visible Absorption, EPR and FTIR Spectroscopies

TSUBAKI, Motonari[1]; MOGI, Tatsushi[2]; HORI, Hiroshi[3]
([1]IMS and Himeji Inst. Tech.; [2]Univ. Tokyo; [3]Osaka Univ.)

[*J. Biochem.* **126**, 510 (1999)]

Cytochrome *bd*-type ubiquinol oxidase contains two hemes *b* (b_{558} and b_{595}) and one heme *d* as the redox metal centers. To clarify the structure of the reaction center, we analyzed *Escherichia coli* cytochrome *bd* by visible absorption, EPR and FTIR spectroscopies using

azide and cyanide as monitoring probes for the exogenous ligand binding site. Azide-binding caused the appearance of a new EPR low-spin signal characteristic of ferric iron-chlorin-azide species and a new visible absorption band at 647 nm. However, the bound azide ($^{14}N_3$) anti-symmetric stretching infrared band (2,010.5 cm^{-1}) showed anomalies upon ^{15}N-substitutions, indicating interactions with surrounding protein residues or heme b_{595} in close proximity. The spectral changes upon cyanide-binding in the visible region were typical of those observed for ferric iron-chlorin species with diol substituents in macrocycles. However, we found no indication of a low-spin EPR signal corresponding to the ferric iron-chlorin-cyanide complexes. Instead, derivative-shaped signals at g = 3.19 and g = 7.15, which could arise from the heme $d(Fe^{3+})$-CN-heme $b_{595}(Fe^{3+})$ moiety,[1)] were observed. After the addition of cyanide, a part of ferric heme *d* showed the rhombic high-spin signal that coexisted with the g_z = 2.85 signal ascribed to the minor heme b_{595}-CN species. This indicates strong steric hindrance of cyanide-binding to ferric heme *d* with the bound cyanide at ferric heme b_{595}.

Reference

1) M. Tsubaki, H. Hori, Mogi, T. Mogi and Y. Anraku, *J. Biol. Chem.* **270**, 28565 (1995).

II-F Structure and Function of Transmembrane Electron Transfer System in Neuroendocrine Secretory Vesicles

In neuroendocrine secretory vesicles of higher animals, intravesicular ascorbate (AsA^-) functions as the electron donor for copper-containing monooxygenases. Upon these monooxygenase reactions, monodehydroascorbate (MDA) radical is produced by oxidation of AsA^-. The MDA radical is reduced back to AsA^- by membrane-spanning cytochrome b_{561} and subsequently the oxidized cytochrome b_{561} is reduced by cytosolic AsA^-. To clarify the molecular mechanism of the electron transfer, we utilize various biophysical techniques (*e.g.* EPR, resonance Raman, and pulse radiolysis) in conjunction with methods of molecular biology and biochemistry. We found previously that purified cytochrome b_{561} from bovine adrenal medulla contains two hemes B per molecule, each exhibiting an independent EPR signal in oxidized state. The reaction of MDA radical with purified cytochrome b_{561} was investigated by the technique of pulse radiolysis. Radiolytically generated MDA radical oxidized rapidly reduced cytochrome b_{561} to yield the oxidized form. Subsequently, the oxidized form was re-reduced by AsA^- in the medium. At excess MDA radical, only half of the heme was oxidized, indicating that only one of the two heme centers can react with MDA radical.

II-F-1 Diethylpyrocarbonate-Modification Abolishes Fast Electron Accepting Ability of Cytochrome b_{561} from AsA^- but Does Not Influence on Electron Donation to MDA Radical: Identification of the Modification Sites by Mass Spectrometric Analyses

TSUBAKI, Motonari[1]; KOBAYASHI, Kazuo[2]; ICHISE, Tomoko[3]; TAKEUCHI, Fusako[3]; TAGAWA, Seiichi[2]

([1]IMS and Himeji Inst. Tech; [2]Osaka Univ.; [3]Himeji Inst. Tech.)

Cytochrome b_{561} in bovine adrenal chromaffin vesicles contains two hemes B[1)] and transports electron equivalents across the vesicle membranes to convert intravesicular MDA radical to AsA^-. To elucidate the mechanism of the transmembrane electron transfer, effects of the treatment of purified cytochrome b_{561} with diethylpyrocarbonate, a reagent specific for histidyl residues, were examined. We found that, when AsA^- was added to the oxidized form of diethylpyrocarbonate-treated cytochrome b_{561}, less than half of the heme iron was reduced but with a very slow rate. In contrast, radiolytically-generated MDA radical was oxidized rapidly by the reduced form of diethylpyrocarbonate-modified cytochrome b_{561}, as observed for untreated cytochrome b_{561}.[2)] These results indicate that the heme center specific for the electron acceptance from AsA^- is perturbed by the modification of amino acid residues nearby. We identified the major modification sites by mass spectrometry at Lys85, His88, and His161, all of which are fully conserved and located at extravesicular side of cytochrome b_{561} in the membranes. We suggest that specific *N*-carbethoxylation of the histidyl ligands of the heme *b* at extravesicular side abolish the electron accepting ability from AsA^-.

References

1) M. Tsubaki, M. Nakayama, E. Okuyama, Y. Ichikawa and H. Hori, *J. Biol. Chem.* **272**, 23206 (1997).
2) K. Kobayashi, M. Tsubaki and S. Tagawa, *J. Biol. Chem.* **273**, 16038 (1998).

II-G Biomolecular Science

Elucidation of a structure-function relationship of metalloproteins is a current subject of this group. The primary technique used for this project is the stationary and time-resolved resonance Raman spectroscopy monitored by near IR to UV lasers. The main themes that we want to explore are (1) mechanism of oxygen activation by enzymes, (2) mechanism of active proton translocation and its coupling with electron transfer, (3) coupling mechanism of proton- and electron transfers by quinones in photosynthetic reaction center, (4) higher order protein structures and their dynamics, and (5) reactions of biological NO. In category (1), we have examined a variety of terminal oxidases, cytochrome P450s, and peroxidases, and also treated their enzymatic reaction intermediates by using the mixed flow transient Raman apparatus and the Raman/absorption simultaneous measurement device. For (2) the third generation UV resonance Raman (UVRR) spectrometer was constructed and we are going to use it to the peroxy and ferryl intermediates of cytochrme c oxidase. In (3) we succeeded in observing RR spectra of quinones A and B in bacterial photosynthetic reaction centers for the first time last year, but we focused our attention on tyrosine radical this year. For (4) we developed a novel technique for UV resonance Raman measuremnts based on the combination of the first/second order dispersions of gratings and applied it successfully to 235-nm excited RR spectra of several proteins including mutant hemoglobins and myoglobins. Nowadays we can carry out time-resolved UVRR experiments with nanosecond resolution to discuss protein dynamics. We have succeeded in isolating the spectrum of β145-Tyr, β35-Tyr and α140-Tyr of Hb A separately and their changes upon quaternary structure transition. For (5) we purified soluble guanylate cyclase from bovine lung and observed its RR spectra. To understand the implication, we examined Raman spectra of NO adducts of various mutant Mbs.

II-G-1 Time-Resolved UV Resonance Raman Detection of a Transient Open Form of the Ligand Pathway in Tyr64(E7) Myoglobin

MUKAI, Masahiro[1]; NAKASHIMA, Satoru[2]; OLSON, John S.[3]; KITAGAWA, Teizo
([1]RIKEN; [2]Osaka Univ.; [3]Rice Univ.)

[*J. Phys. Chem.* **102**, 3624 (1998)]

X-ray crystallographic analyses of myoglobin (Mb) in the deoxy- and CO-bound states noted the absence of a preformed pathway for ligand movement from the heme iron to the solvent. To explore a mechanism of ligand entry, time-resolved UV resonance Raman experiments have been carried out, using a mutant with tyrosine at the distal histidine position. The results indicate the presence of a transient, open pathway which is generated after photodissociation of CO in the H64Y mutant. The Raman spectra were probed at 235 and 416 nm with a time resolution of 7 ns in the range -100 ns to 10 ms following photolysis at 532 nm. In the 235-nm excited spectra, the tyrosine bands of H64Y Mb at 1618 (Y8a) and 1176 cm^{-1} (Y9a) are noticeably intensity-enhanced shortly after photolysis but the original intensity is restored by 5 ms. The time range in which the Tyr bands are intensified is prolonged by addition of glycerol to the solvent. This intensity change is not seen with the native Mb which has three naturally occurring Tyr residues. Thus, the intensity increase observed for the mutant Mb is attributed to Tyr64. The corresponding bands of *para*-cresol derivative exhibit greater intensity in polar (H-bond forming) solvents than in nonpolar solvents. This result suggests that the increase in intensity of the Tyr bands in the transient form of the mutant myoglobin compared to that in the equilibrium form is due to exposure of Tyr64 to solvent water. Increased solvation indicates an outward movement of the phenol side chain and formation of an open channel to the distal pocket.

II-G-2 UV Resonance Raman Studies of α-Nitrosyl Hemoglobin Derivatives: Relation between the α1-β2 Subunit Interface Interactions and the Fe-Histidine Bonding of α Heme

NAGATOMO, Shigenori; NAGAI, Masako[1]; TSUNESHIGE, Antonio[2]; YONETANI, Takashi[2]; KITAGAWA, Teizo
([1]Kanazawa Univ.; [2]Univ. Pennsylvania)

[*Biochemistry* **38**, 9659 (1999)]

Human α-nitrosyl β-deoxy hemoglobin A, $\alpha^{NO}\beta^{deoxy}$, is considered to have a T(tense) structure with the low O_2 affinity extreme and the Fe-histidine(His87) (Fe-His) bond of α heme cleaved. The Fe-His bonding of α heme and the intersubunit interactions at α1-β2 contact of α^{NO}-Hbs have been examined under various conditions with EPR and UV resonance Raman (UVRR) spectra excited at 235 nm, respectively. NOHb at pH 6.7 gave the UVRR spectrum of the R structure, but in the presence of inositol-hexakis-phosphate (IHP) for which the Fe-His bond of the α heme is broken, UVRR bands of Trp residues behaved half T-like while Tyr bands remained in the R-like. The half ligated nitrosylHb, $\alpha^{NO}\beta^{deoxy}$, in the presence of IHP at pH 5.6, gave T-like UVRR spectra for both Tyr and Trp, but binding of CO to its β heme ($\alpha^{NO}\beta^{CO}$) changed the UVRR spectrum to half T-like. Binding of NO to its β heme (NOHb) changed the UVRR spectrum to 70% T-type for Trp but almost R-type for Tyr. When pH was raised to 8.2 in the presence of IHP, the UVRR spectrum of NOHb was the same as that of COHb. EPR spectra of these Hbs indicated that the Fe-His bond of α^{NO} heme is partially cleaved. On the other hand, the UVRR spectra of $\alpha^{NO}\beta^{deoxy}$ in the absence of IHP at pH 8.8 showed the T-like UVRR spectrum but EPR spectrum indicated that 40-50% of the Fe-His bond of α hemes was intact. Therefore, it became evident that there is qualitative correlation between the cleavage of the Fe-His bond of α heme and T-like contact of Trp-β37. We note that the

behaviors of Tyr and Trp residues at the α1-β2 interface are not synchronous. It is likely that the behaviors of Tyr residues are controlled by the ligation of β heme through His-β92(F8) → Val-β98(FG5) → Asp-β99(G1) → Tyr-α42(C7) or Tyr-β145(HC2).

II-G-3 Observation of Cu-N_3^- Stretching and N_3^- Asymmetric Stretching Bands for *mono*-Azide Adduct of *Rhus vernicifera* Laccase

HIROTA, Shun[1]; MATSUMOTO, Hiroki[1]; HUANG, Hong-Wei; SAKURAI, Takeshi; KITAGAWA, Teizo; YAMAUCHI, Osamu[1]
([1]Nagoya Univ.)

[*Biochem. Biophys. Res. Commun.* **243**, 435 (1998)]

Mono-azide adduct of *Rhus vernicifera* laccase, a multicopper oxidase containing one type-1 (blue) copper, one type-2 (non-blue normal) copper, and a pair of type-3 (binuclear and EPR silent) coppers, of which type-2 and type-3 coppers constitute a trinuclear site, was investigated with resonance Raman (RR) and Fourier transform infrared (FT-IR) spectroscopies as a step toward elucidation of the structure and function of the trinuclear site. The Cu-N_3^- stretching ($\nu_{Cu\text{-}N_3^-}$) RR band was observed for azide-bound multicopper oxidases for the first time. The $\nu_{Cu\text{-}N_3^-}$ band was located at 400 cm^{-1} for mono-$^{14}N_3^-$ laccase, which shifted to 396 cm^{-1} with the $^{15}N^{14}N^{14}N_3^-$ analog. The N_3^- asymmetric stretching ($\nu_{(N_3^-)asym}$) band was observed by FT-IR spectroscopy at 2035 cm^{-1} for mono-$^{14}N^{3-}$ laccase and at 2025 cm^{-1} for the $^{15}N^{14}N^{14}N_3^-$ analog. The $\nu_{Cu\text{-}N_3^-}$ and $\nu_{(N_3^-)asym}$ frequencies and their $^{15}N^{14}N$-$^{14}N^-$ isotope shifts for azido laccase correspond well with those of metazido hemocyanin, indicating that both derivatives should have a similar binding geometry of azide.

II-G-4 Studies of Bovine Enterovirus Structure by Ultraviolet Resonance Raman Spectroscopy

KAMINAKA, Shouji[1]; IMAMURA, Yoshihiro[1]; SHINGU, Masahisa[1]; KITAGAWA, Teizo; TOYODA, Tetsuya[1]
([1]Kurume Univ.)

[*J. Virol. Methods* **77**, 117 (1999)]

The structural comparison of bovine enterovirus MZ468 strain before and after the heat treatment was studied by ultraviolet resonance Raman (UVRR) spectra excited at both 235 and 251 nm. The difference between full, heated full and purified empty particles, which were expected as an in vitro model of uncoating, were demonstrated. At 235 nm excitation, the Raman bands of the capsid protein dominated in all the UVRR spectra. The UVRR spectra of the empty particles exhibited non-homogenious broadening for tryptophan W3 band and W7 Fermi doublet bands, which were characteristics of hydrophobic environment, when compared with those of the full particles. The results indicates that some Trp indole rings of the full particles were packaged inside the viral capsids and not strained by virion assembly. On the other hand, the Raman bands assigned to guanine residues of the single stranded-RNA genome were enhanced strongly in the 251-nm excited UVRR spectrum. The spectral differences between the packaged (full particles) and the unpackaged virions (heated full particles) indicates that some guanine residues had strong hydrogen bonds in the full particles.

II-G-5 Spectroscopic Characterization and Kinetic Studies of a Novel Plastocyanin from the Green Alga *Ulva pertusa*

SASAKAWA, Yuki[1]; ONODERA, Kazuhiko[1]; KARASAWA, Machiko[1]; IM, Sang-Choul[1]; SUZUKI, Eiji[1]; YOSHIZAKI, Fuminori[2]; SUGIMURA, Yasutomo[2]; SHIBATA, Naoki[3]; INOUE, Tsuyoshi[3]; KAI, Yasushi[3]; NAGATOMO, Shigenori; KITAGAWA, Teizo; KOHZUMA, Takamitsu[1]
([1]Ibaraki Univ.; [2]Toho Univ.; [3]Osaka Univ.)

[*Inorg. Chim. Acta* **283**, 184 (1998)]

A novel plastocyanin from the green alga *Ulva pertusa* was isolated and characterized. The electronic absorption and the electron paramagnetic resonance spectroscopic properties of *Ulva* plastocyanin showed features characteristic of the usual plastocyanins reported so far. However, the resonance Raman spectrum on excitation at 607 um indicated the Raman band of Cu-S_{cys} at 413 cm^{-1}; this is at a lower frequency than the corresponding Raman band of higher plant plastocyanins. Electron-transfer reactions were investigated with $[Fe(CN)_6]^{3-}$ and $[Co(phen)_3]^{3+}$ complexes. The electron-transfer rate constant of *Ulva* plastocyanin was determined to be $(1.18 \pm 0.06) \times 10^5$ $M^{-1}s^{-1}$ for the reaction with $[Fe(CN)_6]^{3-}$ at pH 7.5, and the intramolecular electron-transfer rate constant and equilibrium constant for complex formation for the reaction with $[Co(phen)_3]^{3+}$ were evaluated to be 7.7 ± 0.6 s^{-1} and $(4.2 \pm 0.4) \times 10^2$ M^{-1} respectively. The electron-transfer rate constant for the reaction with $[Fe(CN)_6]^{3-}$ at pH 7.5 is two times larger than the values obtained from the other higher plant plastocyanins. The kinetic behavior suggested that the structure is slightly different from those of other plastocyanins. It has been reported that the electron-transfer reaction of plastocyanin is inhibited by the protonation of the active site histidine (His87 in poplar plastocyanin) at acidic pH. The dependence on pH of the rate constant for the reaction with $[Fe(CN)_6]^{3-}$ was investigated. The acid-dissociation constant accompanying the electron-transfer reaction was determined to be $pK_H = 5.8$. Second-order rate constants for the reduction of plastocyanin by cytochrome c were determined to be $(1.71 \pm 0.04) \times 10^6$ $M^{-1}s^{-1}$ at $I = 0.1$ M (NaCl), pH 7.0 (20 mM Tris-HCl buffer). The saturation kinetic behavior for the reaction was not observed even at the lower ionic strength (20 mM Tris-HCl).

II-G-6 Aliphatic Hydroxylation by a Bis(μ-Oxo)-Dinickel(III) Complex

ITOH, Shinobu[1]; BANDOH, Hideki[1]; NAGATOMO, Shigenori; KITAGAWA, Teizo; FUKUZUMI, Shunichi[1]

([1]Osaka Univ.)

[*J. Chem. Soc.* in press]

Treatment of $[(\mathbf{L}^{X}Ni^{II})_2(\mu\text{-}OH)_2]^{2+}$ ($\mathbf{L}^{X}$ = *p*-substituted *N*,*N*-bis[2-(2-pyridyl)ethyl]-2-phenylethylamine; X = OMe, Me, H, Cl) with one equivalent of H_2O_2 gave a bis(μ-oxo)dinickel(III) complex, $[(\mathbf{L}^{X}Ni^{III})_2(\mu\text{-}O)_2]^{2+}$, the formation of which has been confirmed by a characteristic absorption band at 408 nm (ε = 6000 $M^{-1}cm^{-1}$) and a resonance Raman band at 612 cm^{-1} that shifts to 580 cm^{-1} upon ^{18}O-substitution. The bis(μ-oxo)-dinickel(III) complex gradually decomposes to lead to benzylic hydroxylation of the ligand side arm (phenethyl group). Rates of the formation and decay of the bis(μ-oxo)dinickel(III) complex were determined directly by monitoring the absorption change at 408 nm at low temperatures. The kinetic data of the ligand hydroxylation process including kinetic deuterium isotope effect (KIE), p-substituent effects (Hammett plot), and activation parameters ($\Delta H^{\neq}$ and $\Delta S^{\neq}$) have indicated that the bis(μ-oxo)dinickel(III) complex behaves as an electrophilic radical as in the case of bis-(μ-oxo)dicopper(III) complexes.

II-G-7 The Structure and Unusual pH Dependence of Plastocyanin from the Fern Dryopteris Crassirhizoma: The Protonation of an Active Site Histidine is Hindered by π-π Interactions

KOHZUMA, Takamitsu[1]; INOUE, Tsuyoshi[2]; YOSHIZAKI, Fuminori[3]; SASAKAWA, Yuki[1]; ONODERA, Kazuhiko[1]; NAGATOMO, Shigenori; KITAGAWA, Teizo; UZAWA, Sachiko[3]; ISOBE, Yoshiaki[3]; SUGIMURA, Yasutomo[3]; GOTOWDA, Masaharu[2]; KAI, Yasushi[2]
([1]Ibaraki Univ.; [2]Osaka Univ.; [3]Toho Univ.)

[*J. Biol. Chem.* **274**, 11817 (1999)]

Spectroscopic properties, amino acid sequence, electron transfer kinetics, and crystal structures of the oxidized (at 1.7 Å resolution) and reduced form (at 1.8 Å resolution) of a novel plastocyanin from the fern *Dryopteris crassirhizoma* are presented. Kinetic studies show that the reduced form of *Dryopteris* plastocyanin remains redox-active at low pH under conditions where the oxidation of the reduced form of other plastocyanins is inhibited by the protonation of a solvent-exposed active site residue, His87 (equivalent to His90 in *Dryopteris* plastocyanin). The x-ray crystal structure analysis of *Dryopteris* plastocyanin reveals π-π stacking between Phe12 and His90, suggesting that the active site is uniquely protected against inactivation. Like higher plant plastocyanins, *Dryopteris* plastocyanin has an acidic patch, but this patch is located closer to the solvent-exposed active site His residue, and the total number of acidic residues is smaller. In the reactions of *Dryopteris* plastocyanin with inorganic redox reagents, the acidic patch (the "remote" site) and the hydrophobic patch surrounding His90 (the "adjacent" site) are equally efficient for electron transfer. These results indicate the significance of the lack of protonation at the active site of *Dryopteris* plastocyanin, the equivalence of the two electron transfer sites in this protein, and a possibility of obtaining a novel insight into the photosynthetic electron transfer system of the first vascular plant fern, including its molecular evolutionary aspects. This is the first report on the characterization of plastocyanin and the first three-dimensional protein structure from fern plant.

II-G-8 Model Complexes of the Active Form of Galactose Oxidase. Physicochemical Properties and Reactivity of Cu(II)- and Zn(II)- Phenoxyl Radical Complexes of the Novel Organic Cofactor

ITOH, Shinobu[1]; TAKI, Masayasu[1]; KUMEI, Hideyuki[1]; TAKAYAMA, Shigehisa[1]; NAGATOMO, Shigenori; KITAGAWA, Teizo; SAKURADA, Norio[2]; ARAKAWA, Ryuichi[2]; FUKUZUMI, Shunichi[1]
([1]Osaka Univ.; [2]Kansai Univ.)

[*Angew. Chem., Int. Ed. Engl.* in press]

Model complexes of the active sites of galactose oxidase (GAO) and glyoxal oxidase (GLO) have been prepared using new cofactor models, 2-methylthio-4-*tert*-butyl-6-[[bis[2-(2-pyridyl)ethyl]amino]methyl]-phenol (**1H**) and 2,4-di-*tert*-butyl-6-[[bis[2-(2-pyridyl)-ethyl]amino]methyl]phenol (**2H**). Deprotonated ligand $\mathbf{1}^{-}$ forms dimeric Cu(II)-and Zn(II)-complexes, $[Cu^{II}_2(\mathbf{1}^{-})_2](PF_6)_2$ and $[Zn^{II}_2(\mathbf{1}^{-})_2](PF_6)_2$, in the solid state, but those complexes were converted into the monomers, $[Cu^{II}(\mathbf{1}^{-})(AcO^{-})]$ and $[Zn^{II}(\mathbf{1}^{-})(CH_3CN)]^{+}$, in solution by the coordination of acetate ion and CH_3CN, respectively. On the other hand, $\mathbf{2}^{-}$ forms monomeric Cu(II)- and Zn(II)-complexes, $[Cu^{II}(\mathbf{2}^{-})(CH_3CN)]PF_6$ and $[Zn^{II}(\mathbf{2}^{-})(CH_3CN)]PF_6$, both in the solid state and in solution. The structures and the physical properties of the Cu(II)- and the Zn(II)-complexes of the phenolate derivatives ($\mathbf{1}^{-}$ and $\mathbf{2}^{-}$) have been explored as the models for the resting sate of the enzymes. Oxidation of the Cu(II)- and Zn(II)-complexes of $\mathbf{1}^{-}$ and $\mathbf{2}^{-}$ by $(NH_4)_2[Ce^{IV}(NO_3)_6]$ (CAN) affords the corresponding phenoxyl radical complexes, $[M^{II}(\mathbf{1}^{\bullet})(NO_3^{-})]^{+}$ and $[M^{II}(\mathbf{2}^{\bullet})(NO_3^{-})]^{+}$ (M = Cu and Zn), the electronic structures and the physicochemical properties of which have been examined by UV-vis, resonance Raman, ESI-MS, and ESR. The radical complexes $[M^{II}(\mathbf{1}^{\bullet})(NO_3^{-})]^{+}$ are relatively stable at ambient temperature to show very broad absorption bands in the long wavelength region (λ_{max} = 867 and 887 nm for Cu(II)- and Zn(II)-complexes, respectively) as observed for the *active form* of the native enzymes. The Cu(II)-phenoxyl radical complexes oxidize benzyl alcohol derivatives to benzaldehydes quantitatively via a formal $2e^{-}/2H^{+}$ mechanism, where the Cu(II)-phenoxyl radical complexes are converted into the corresponding Cu(I)-phenol complexes. On the other hand, oxidation of benzyl alcohols by the Zn(II)-phenoxyl radical complexes requires two equivalents of the radical complex per alcohol, indicating that the redox reaction takes place only at the phenoxyl radical site in a dimeric form. Such a difference in the reactivity between the

Cu(II)- and the Zn(II)-complexes clearly demonstrates the importance of the redox cycle between Cu(I) and Cu(II) as well as the interconversion between the phenol and phenoxyl radical froms for the efficient two-electron oxidation of alcohols at the *mononuclear copper site* of GAO. Substituent effects of the thioether group on the reactivity are also discussed in relation with the physicochemical properties of the Cu(II)- and Zn(II)-phenoxyl radical complexes.

II-G-9 A Bis(μ-Oxo)Dicopper(III) Complex with Sterically Hindered Aromatic Nitrogen Donors: Structural Characterization and Reversible Conversion between Copper(I) and Bis(μ-Oxo)-Dicopper(III) Species

HAYASHI, Hideki[1]; FUJINAMI, Shuhei[1]; NAGATOMO, Shigenori; OGO, Seiji; SUZUKI, Masatatsu[1]; UEHARA, Akira[1]; WATANABE, Yoshihito; KITAGAWA, Teizo
([1]Kanazawa Univ.)

[*J. Am. Chem. Soc.* in press]

Recently, Tolman *et al.* and Stack *et al.* have prepared high-valent $Cu(III)_2(\mu\text{-}O)_2$ species generated by the O-O bond scission of O_2^{2-}- which exhibited monooxygenase activity. Crystallographically characterized bis(μ-oxo)dicopper(III) complexes reported so far consist of tridentate or bidentate aliphatic nitrogen donors. It is important to explore how the nature of donor atoms and the stereochemistry of ligands influence the structures and properties of bis(μ-oxo)-dicopper(III) complexes. In this context, we have synthesized a bis(μ-oxo)dicopper(III) complex, $[Cu_2(O)_2(Me_2\text{-tpa})_2](PF_6)_2\cdot 2(CH_3)_2CO$ (**1b**), having a tetradentate tripodal ligand containing aromatic nitrogen donors. Complex **1b** is the first crystallographically characterized bis(μ-oxo)dicopper(III)) complex having

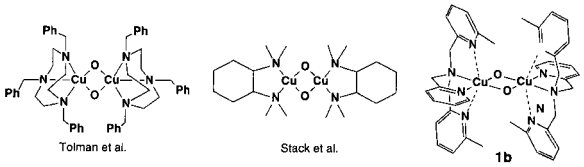

aromatic nitrogen donors.

The most striking feature of **1b** is the reversible conversion with a precursor copper (I) complex $[Cu(Me_2\text{-tpa})]^+$ (**1a**) in CH_2C1_2 at –80 °C by bubbling N_2 gas. Such reversible behavior has not been observed for the bis(μ-oxo)dicopper(III) complexes. Complex **1b** exhibited monooxygenase activity for the Me_2-tpa ligand to produce a N-dealkylated product, (6-methyl-2-pyridylmethyl)(2-pyridylmethyl)amine together with 6-methylpyridine-2-carbaldehyde in which oxygen atom comes from dioxygen. The results indicate that N-dealkylation appears to proceed through oxygen atom transfer from the bridging oxo group to the methylene carbon atom of the 6-methyl-2-pyridylmethyl side arm.

II-H Fast Dynamics of Photoproducts in Solution Phases

Picosecond time-resolved resonance Raman (ps-TR^3) spectroscopy is a promising technique to investigate ultrafast structural changes of molecules. However, this technique has not been used as widely as nanosecond TR^3 spectroscopy, mainly due to the lack of light source which has suitable repetition rates of pulses and wavelength tunability. In order to obtain qualified TR^3 spectra, first we need two independently tunable light sources for pump and probe pulses. Second, the repetition rate should be higher than kilohertz to keep a moderate average laser power without allowing the photon density of probe pulse too high. We succeeded in developing light sources for ps-TR^3 spectroscopy having wide tunability and kHz repetition, and applied them to study fast dynamics of photo-excited molecules. For carbonmonoxy myoglobin (MbCO), vibrational relaxation with the time costant of 1.9 ps was observed for CO-photodissociated heme. For Ni-octaethylporphyrin in benzene, differeces in rise times of population in vibrationally excited levels among various modes were observed in the anti-Stokes spectra for the first time. For the same molecule in piperidine, coordination of two solvent molecules was observed in the transient (*d,d*) excited state. The ps-TR^3 experiments were also applied to Zn-porphyrin dimers, for which some evidence for the π-π interaction in the S_1 state was obtained. The UV ns-TR^3 experiments on MbCO demonstrated the presence of a transient open form of the ligand pathway.

II-H-1 Intramolecular Vibrational Energy Redistribution and Intermolecular Energy Transfer in the (*d,d*) Excited State of Nickel Octaethylporphyrin

MIZUTANI, Yasuhisa; UESUGI, Yuki; KITAGAWA, Teizo

[*J. Chem. Phys.* **111**, 8950 (1999)]

The formation of a vibrationally excited photoproduct of nickel octaethylporphyrin (NiOEP) upon (π,π*) excitation and its subsequent vibrational energy relaxation were monitored by picosecond time-resolved resonance Raman spectroscopy. Stokes Raman bands due to the photoproduct instantaneously appeared upon the photoexcitation. Their intensities decayed with a time constant of ~300 ps, which indicates electronic relaxation from the (*d,d*) excited state (B_{1g}) to the ground state (A_{1g}), being consistent with the results of transient absorption measurements by Holten and coworkers [D. Kim, C. Kirmaier and D. Holten, *Chem. Phys.* **75**, 305 (1983); J. Rodriguez and D. Holten, *J. Chem. Phys.* **91**, 3525 (1989)]. The Raman frequencies of NiOEP in the (*d,d*) excited state are shifted to lower frequencies compared to those of the ground state species, and it is reasonably interpreted by the core size expansion of the macrocycle by 0.05 Å upon the

electron promotion from the d_{z^2} to the $d_{x^2-y^2}$ orbital. Anti-Stokes ν_4 intensity in vibrationally excited (*d*,*d*) state of NiOEP appeared promptly and decayed with time constants of 11 ± 2 and 330 ± 40 ps. The former is ascribed to vibrational relaxation, while the latter corresponds to the electronic relaxation from the (*d*,*d*) excited state to the electronic ground state. In contrast, the rise of anti-Stokes ν_7 intensity was not instantaneous, but delayed by 2.6 ± 0.5 ps, which indicates that intramolecular vibrational energy redistribution has not been completed in subpicosecond time regime. The peak position of ν_4 band shifted by nearly 5 cm^{-1} between 0 and 50 ps. The time constant for the shift of the ν_4 band was 9.2 ± 1.3 ps, which was close to that for the fast component of intensity decay of anti-Stokes bands. The ν_4 band became narrower and symmetric as the delay time increases. These can be ascribed to intramolecular anharmonic coupling of the ν_4 mode with the low frequency modes which can exchange energy with solvent molecules. The intra- and intermolecular vibrational energy relaxation in the metal excited state will be discussed.

II-H-2 Time-Resolved Resonance Raman Study of Intermediates Generated after Photodissociation of Wild-type and Mutant CO-Myoglobins

NAKASHIMA, Satoru[1]; KITAGAWA, Teizo; OLSON, John S.[2]
([1]Osaka Univ.; [2]Rice Univ.)

[*Chem. Phys.* **228**, 323 (1998)]

Time-resolved resonance Raman (TR^3) spectroscopy was applied to elucidate transient structures of myoglobin (Mb) involved in its ligand binding. Pump/probe Raman measurements of the Fe-CO stretching bands ($\nu_{Fe\text{-}CO}$) were carried out for various delay times (Δt = –20 ns – 1 ms with a time resolution of 7 ns) after laser photolysis of native and mutant COMb complexes. His64(E7) and Leu29(B10) were replaced with an aliphatic and aromatic residues. The static $\nu_{Fe\text{-}CO}$ frequencies of the mutants depended strongly on the environments around the bound CO and correlated more with the hydropathy indices of the replaced residues than with their sizes. The kinetics of bimolecular CO recombination correlate with the static $\nu_{Fe\text{-}CO}$ frequencies; a lower frequency generally results in faster rebinding. Despite these differences, all the proteins exhibited the shift of a porphyrin band from 370 to 379 cm^{-1} upon binding of CO and also a transient Raman band at ~497 cm^{-1}, which occurred before recovery of the original $\nu_{Fe\text{-}CO}$ band. The latter frequency was unaffected by isotopically labeling the ligand with $^{13}C^{18}O$. The 497 cm^{-1} band was absent in the spectrum at Δt = 0 ns for all of the myoglobins examined except for the His64 → Leu (H64L) mutant which shows the band immediately after photolysis. The 370 and 497 cm^{-1} bands are associated with the $C_\beta C_c C_d$ in-plane bending of the propionic side chains and the out-of-plane γ_{12} containing pyrrole swiveling and propionic bending motions, respectively. The 497 cm^{-1} transient band appears to reflect a deoxyheme intermediate in which the hydrogen bonding lattice between Arg45(CD3), His64(E7), the heme-6-propionate, and an external distal pocket water molecule is temporarily disrupted. This disruption allows larger movements of the propionate side chain, explaining intensity enhancement of the 497 cm^{-1} band. Recovery of the hydrogen bonding lattice dampens the movements of the propionate $C_\beta C_c C_d$ bond system and finally fixes it in the heme plane in the CO-bound form, causing the frequency shift of the bending mode from 370 cm^{-1} back to 379 cm^{-1}. In the Leu64 mutant, the external water molecule is already absent, facilitating rapid movement of the heme-6-propionate after photolysis. Larger scale movements of all three side chains could create an open conformation with a channel from the heme iron to the solvent, allowing ligand escape and/or rebinding.

II-H-3 Characterization of Stimulated Raman Scattering of Hydrogen and Methane Gases as a Light Source of Picosecond Time-Resolved Raman Spectroscopy

UESUGI, Yuki; MIZUTANI, Yasuhisa; KRUGLIK, Sergei G.[1]; SHVEDKO, Alexander G.[1]; ORLOVICH, Valentin A.[1]; KITAGAWA, Teizo
([1]Natl. Acad. Sci. Belarus)

[*J. Raman Spectrosc.* in press]

Stimulated Raman scattering (SRS) in compressed hydrogen and methane gas has been characterized in terms of pulse energy, temporal width, and spectral width in the range of gas pressures of 10–60 atm. to use it as a light source of picosecond time-resolved resonance Raman spectroscopy. SRS was pumped by the second harmonic of a Ti:sapphire oscillator-regenerative amplifier laser system with pulse energy up to 200 μJ, duration of ~2.5 ps and repetition rate of 1 kHz. The output spectral region of 421–657 nm was covered by the first and second Stokes SRS components on tuning of the pump wavelength in the range of 375–425 nm, Energy conversion to the first Stokes SRS component was more than 10% with H_2 and more than 20% with CH_4. The temporal width of SRS-pulse (1.1–2.1 ps) was shorter than that of a pump pulse. Spectral band shape was found to be modulated, since the SRS is generated in a transient regime. When more than 100 pulses were averaged over, the temporal and spectral profiles of SRS-pulses were sufficiently smooth and energy fluctuations were sufficiently small for spectroscopic applications. On the basis of the results obtained, an optimized condition as a Raman shifter was settled. The Raman shifter served as a light source for two-color pump-probe time-resolved resonance Raman (TR^3) experiments and to demonstrate its capabilities, picosecond TR^3 spectra of nickel tetraphenylporphyrin in toluene solution have been measured.

II-H-4 Nanosecond Temperature Jump and Time-Resolved Raman Study of Thermal Unfolding of Ribonuclease A

YAMAMOTO, Kohji[1]; MIZUTANI, Yasuhisa;

KITAGAWA, Teizo
([1]GUAS)

A nanosecond temperature jump (T-jump) apparatus heating at 1.56 μm was constructed and combined with time-resolved Raman measurements to investigate thermal unfolding of a protein for the first time. The 1.56 μm-heat pulse with 9 ns width was obtained through the two-step stimulated Raman scattering in D_2 gas involving seeding and amplification excited by the fundamental (1064 nm) of a Nd:YAG laser. The energy of the heiat pulse was 135 mJ at 10 Hz repetition when the power of the 1064 nm-input was 560 mJ, and the pulse-to-pulse fluctuation was less than 10%. To achieve uniform temperature rise in the illuminated part, the counter-propagation geometry was adopted. The magnitude of temperature rise was determined by anti-Stokes to Stokes Raman intensity ratio of the 317 and 897 cm^{-1} bands of MoO_4^{2-} aqueous solution measured at various delay times with the second harmonic (532 nm) of another Nd:YAG laser. The T-jump as large as 9 °C was attained within the temporal width of the heat pulse. The thermal unfolding of bovine pancreatic ribonuclease A (RNase A) was monitored with time-resolved Raman spectroscopy following T-jump with this apparatus. In the initial 200 ns after T-jump, the C-S stretching Raman band of methionine residues exhibited 10% change of that expected from the steady state spectra and another 10% in 5 ms. The Raman intensity of SO_4^{2-} ions around 980 cm^{-1} increased and was shifted to a lower frequency than the steady state frequency of the elevated temperature at 100 μs delay, presumably due to partial release from the active site. The Raman bands of S-S stretches and tyrosine doublets displayed little change within 5 ms, although appreciable changes were expected from the steady state spectra. Thus, it has been demonstrated for the first time for proteins that the combination of laser T-jump with time-resolved Raman spectroscopy will serve as a powerful tool for studies of thermal unfolding and that the conformation change in the initial step of unfolding is not always concerted.

II-H-5 Evidence for π-π Interactions in the S_1 State of Zn Porphyrin Dimers Revealed by Picosecond Time Resolved Resonance Raman Spectroscopy

NAKASHIMA, Satoru[1]; TANIGUCHI, Seiji[1]; OKADA, Tadashi[1]; OSUKA, Atsuhiro[2]; MIZUTANI, Yasuhisa; KITAGAWA, Teizo
([1]Osaka Univ.; [2]Kyoto Univ.)

[*J. Phys. Chem. A* in press]

The S_1 states of Zn(II) porphyrin dimers have been investigated with picosecond time-resolved resonance Raman spectroscopy. The transient absorption and Raman spectra of porphyrin dimers, in which two Zn(II)-porphyrins are covalently linked at the *ortho* or *meta* positions of phenylene spacers, are compared with those of their component monomer unit. Although Q-band of the *ortho* dimer was definitely different from those of the *meta* dimer and reference monomer, the ground state Raman spectra of the *ortho* and *meta* dimers are nearly the same as that of monomer, suggesting that the porphyrin π-π interactions do appear in the excited state of the *ortho* dimer but little in the ground state. Several characteristic Raman bands were observed for the S_1 excited state at 2 ps after photo-excitation. The monomer in the S_1 state gave the marker bands at slightly lower frequencies (by 3–4 cm^{-1}) than the corresponding ground state molecules and they did not show frequency shifts with time between 2 and 300 ps. On the contrary, in the case of the *ortho* dimer, two characteristic bands (ν_2, ν_4) appeared at frequencies significantly lower (by 10–13 cm^{-1}) than the corresponding ground state bands, and in addition the frequency of ν_4 band exhibited an upshift around 10–20 ps following photoexcitation. The frequency shift of the *ortho* dimer was appreciably perturbed by steric hindrance between the two porphyrin groups introduced through bulky *tert*-butyl group at *para* position. The behaviors of transient Raman bands of the meta dimer appeared intermediate between the monomer and the *ortho* dimer. These observations give the first clear evidence for the presence of π-π interactions in the S_1 excited state of porphyrin dimers with phenylene spacer and the occurrence of relaxation toward the monomer-type structure in several tens picoseconds.

II-I Molecular and Electronic Structures of Metallofullerenes and the Fullerene Radical Anions

The continued interest in radical ions of fullerenes and metallofullerenes has resulted from the discovery of superconductivity in the CT complexes of alkali metals with fullerenes. Spectroscopic information concerning the electronic and spin states of the metallofullerenes has been obtained by EPR and ENDOR measurements.

II-I-1 Spin Chemistry of Metallofullrenes

KATO, Tatsuhisa; OKUBO, Shingo; AKASAKA, Takeshi[1]
([1]Niigata Univ.)

The consideration of crystal field effect due to the fullerene cage with the low symmetry was indispensable for the analysis of the electronic and spin states for the metal ion encapsulated inside the fullerene cage. The ESR spectrum of $Gd@C_{82}$ could not be reproduced by the simulation without the assumption of the crystal field splitting of the ground electronic state. The ESR spectrum of $Pr@C_{82}$ exhibited no resolved band, this result could be also explained by the crystal filed splitting.

II-J Site Selective Spectroscopy in Solid Crystals

The line broadening due to the variation of the environment over the some sites in the crystal structure prevents from determining small energy splitting between pair of closely spaced levels with high accuracy. However the broadening effects give a nice prove to investigate the intermolecular interaction in the crystal structure. On the other hand some techniques of the site selective spectroscopy to eliminate the disturbance were proposed. We are applying the technique of the heterodyne detection of optical magnetic double-resonance to some systems of crystal.

II-J-1 NQR by Coherent Raman Scattering of a Triplet Exciton in a Molecular Crystal

MATSUSHITA, Michio; KATO, Tatsuhisa

[*Phys. Rev. Lett.* **83**, 2018 (1999)]

Nuclear quadrupole resonance (NQR) of a linear triplet exciton in 1,4-dibromonaphthalene crystals has been observed as coherent Raman scattering. The Br NQR scattering originates from the hyperfine interaction between the electron spin and the Br spins. Since delocalization of the electron spin decreases the interaction, the intensity of the NQR scattering reflects the chain length of the exciton. The exciton is found to be delocalized over about 10 molecules, indicating the coherence length of the exciton is limited by scattering due to ^{13}C isomers.

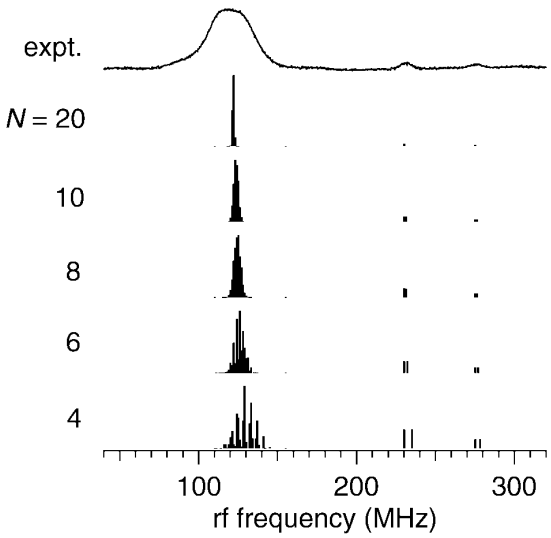

Figure 1. Coherent Raman spectrum calculated for the exciton in 1,4-DBN delocalized over *N* molecules. The result is shown as histograms of the width of 1 MHz. The observation is shown on the top for the sake of comparison.

II-K State Correlated Raman Spectroscopy

The vibrational Raman polarizability tensor responds to molecular reorientational relaxation process, and the structural environment in condensed media. The measurement of Raman scattering is a powerful technique for the study of molecular motion and of the mechanism of phase transition. We've built up the system of multichannel type detection of Raman scattering combined with the temperature controlled cell.

II-K-1 An Analysis of Polarized Raman Scattering Measurements for the Orientational Ordering of Ferro- and Antiferroelectric Liquid Crystal

HAYASHI, Naoki; KATO, Tatsuhisa

The orientational ordering of the ferro- and antiferroelectric liquid crystal molecule, MHPOBC was investigated in the series of the successive smectic phases by means of the polarized Raman scattering measurement. The improved equation of the polarized Raman intensity was derived as a function of the orientational order parameter and the incident laser polarization. According to the equation the second and the fourth orientational order parameters, $\langle P_2 \rangle$ and $\langle P_4 \rangle$, could be evaluated even in the chiral smectic phases. An unusual change of the orientational order parameter was observed with decreasing of temperature as shown in Figure 1. It was concluded that the irregular variation of the order parameter stemed from the biaxiality of the molecular orientational distribution. It could be attributed to the difference of the angle between the optical axis and the center axis of the molecular orientational distribution as the increasing of biaxiality.

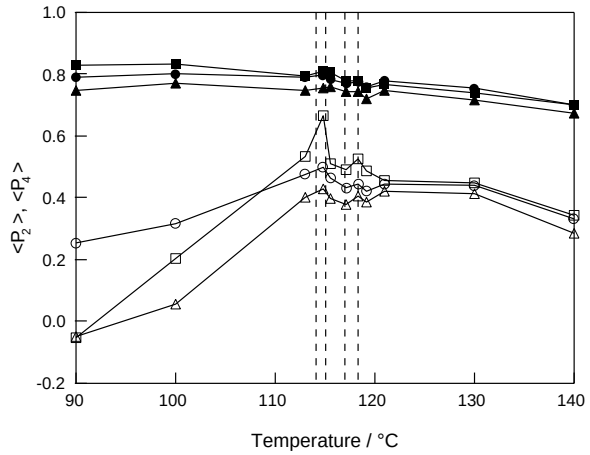

Figure 1. Temperature dependence of the orientational order parameter, $\langle P_2 \rangle$ (solid circle: phenyl, solid square: chiral C=O, solid triangle: core C=O) and $\langle P_4 \rangle$ (open circle: phenyl, open square: chiral C=O, open triangle: core C=O). The broken lines show the phase transition points. The phase sequence is as SmA-SmC_α*-SmC*- SmC_γ*-SmC_A*.